Accurate Representations of the Microphysical Processes Occurring During the Transport of Exhaled Aerosols and Droplets

Jim S. Walker,[1] Justice Archer,[1] Florence K. A. Gregson[1], Sarah E. S. Michel[1], Bryan R. Bzdek[1] and Jonathan P. Reid[1,*]

[1] School of Chemistry, University of Bristol, Bristol, BS8 1TS

1. Experimental Methods

We measure the evaporation kinetics and hygroscopicity of droplets containing artificial saliva (AS) as well as those containing surrogate deep lung fluid (DLF) using a Comparative-Kinetics Electrodynamic Balance (CK-EDB). This instrument has been used to measure the hygroscopicity of inorganic,[1] organic,[2] and mixed aerosol,[3] as well as to record droplet evaporation kinetics.[4,5] Thus, the techniques are described in previous publications and will only be briefly reviewed here. No unexpected or unusually high safety hazards were encountered.

A single charged droplet ($r \sim 25$ μm) is produced by a droplet-on-demand generator (MicroFab MJ-APB-01, orifice diameter 30 μm). The droplet is of known composition and is charged upon generation in the presence of an induction electrode (< 10 fC) due to an ion imbalance of e.g. OH^- and H_3O^+. The droplet is dispensed into the centre of the CK-EDB instrument and becomes trapped in the null point of an electrodynamic field generated by ac voltage applied to the upper and lower sets of concentric cylindrical electrodes that are mounted vertically opposite one another. An additional dc voltage is applied to the lower sets of electrodes to offset the gravitational and drag forces acting on the droplet. The RH in the CK-EDB can be controlled by adjusting the ratio between dry and wet N_2 gas-flows, that are combined and applied across the droplet at a rate of 0.03 m s^{-1} (RH range of <10 – > 90 %). The temperature in the CK-EDB chamber can be controlled (from 273 K to 323 K) by a circulating polyethylene glycol coolant that passes across the electrodes, and is controlled using a commercial chiller (F32-ME, Julabo). The temperature of the chamber is measured using a K-type thermocouple (National Instruments).

The trapped droplet is illuminated with a 532 nm continuous-wave laser (Laser Quantum, Ventus). A characteristic angularly-resolved elastic light scattering pattern comprising bright and dark fringes (phase function) is observed due to the interference between reflection and refraction of the laser light at the droplet surface. The phase function is collected in the near forward scattering direction at 45 ° by a CCD camera over an angular range of ~ 26 °. The droplet radius, r, can be estimated from the phase function using the geometric optics approximation to Mie theory:

$$r = \frac{\lambda}{\Delta\theta}\left(\cos\left(\frac{\theta}{2}\right) + \frac{m\sin\left(\frac{\theta}{2}\right)}{\sqrt{1 + m^2 - 2\,m\cos\left(\frac{\theta}{2}\right)}}\right)^{-1} \qquad \text{(S1)}$$

where λ is the laser wavelength, $\Delta\theta$ is the average angular spacing between the peaks in the phase function, m is the droplet refractive index, θ is the central viewing angle. This approach estimates the radius of the droplet to an accuracy of ± 100 nm.

The refractive index, m, for an aqueous solution changes throughout the evaporation process due to the compositional change arising from solvent loss. During data acquisition the droplet radius is estimated from the average fringe separation using Eq. S1 in real-time with an initial m of 1.335, i.e. that of water. In a post-data-processing step the droplet radius is corrected for a changing m by estimating the time-dependent mass fraction of solute (*mfs)* and applying the molar refraction mixing rule.[6] The accuracy of this mixing rule to

describe the refractive index of mixtures has been validated experimentally for both inorganic and organic aerosol systems.[3,7] The post-processing step of correcting the raw radius data due to the changing refractive index is described in more detail in a previous publication.[1]

To record the RH in the chamber at the time of a droplet evaporation process, the Comparative Kinetics approach is used.[1] The evaporation kinetics of a pure water probe droplet (for RHs > 80%) are simulated using the Kulmala model and compared with that of a probe droplet produced by a separate droplet-on-demand generator directly prior to the generation of the droplet of interest (See Fig. S1).[8]

The Kulmala model relates the mass flux from a spherical solution droplet in the continuum regime to the difference between the gas phase RH and the water activity at the droplet surface (a_w):

$$I = -2\,Sh\,\pi\,r\,(RH - a_{\mathrm{w}}) \times \left[\frac{R\,T_\infty}{M\,\beta_{\mathrm{M}}\,D\,p^0(T_\infty)\,A} + \frac{a_{\mathrm{w}}\,L^2\,M}{K\,R\,\beta_{\mathrm{T}}\,T_\infty{}^2}\right]^{-1} \qquad \text{(S2)}$$

where R is the ideal gas constant, M is the molar mass of water, D is the mass diffusion coefficient of water vapour, $p^0(T_\infty)$ is the saturation vapour pressure of water at gas phase temperature T_∞. Sh is the Sherwood number, A is a correction for Stefan flow, L is the latent heat of vaporisation of water, K is the thermal conductivity of the gas phase, and β_M and β_T are the transitional correction factors for mass and heat transfer, respectively. A simulation of the evaporation of a probe droplet is performed using Eq. S2, with the RH iterated until the simulation matches the experimental data. The evaporation rate of the simulation (dr^2/dt) is compared with the experimental data to find the RH at which there is the lowest mean squared difference (MSD) between the two profiles (Fig. S1b).

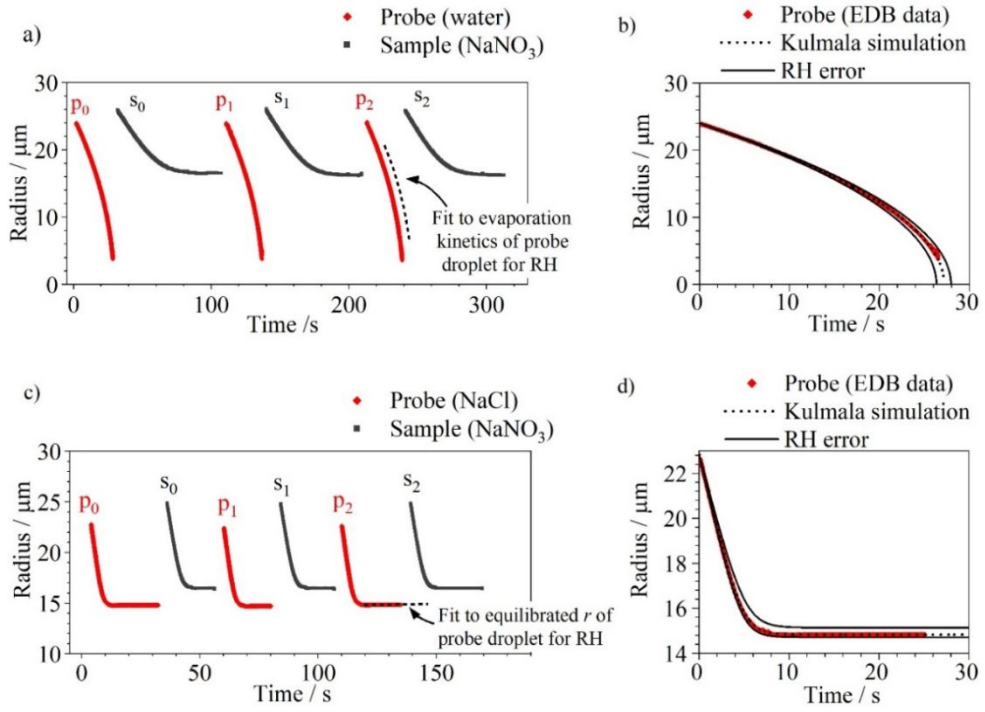

Figure S1: An example of the sequence of probe and sample droplets evaporated in the EDB, used to measure the hygroscopicity of a sample droplet (here $NaNO_3$). In a) The RH is 92% at 293 K, so the probe droplet consists of water, and an example of the Kulmala simulation to fit to the probe droplet evaporation data is

shown in panel b) as the dotted line, with the filled line showing the ± error in the RH retrieval. In c) the RH is 68% at 293 K so an aqueous NaCl solution is used for the probe droplets, with the comparison between the Kulmala simulation and the EDB data shown in panel d).

For an aqueous NaCl probe droplet (for RHs 45% - 80%) the RH is determined using the equilibrated size of the probe droplet following water evaporation (r_{wet}) (Fig. S1d). The ratio between the equilibrated size of the probe droplet and the dry radius of pure NaCl in the particle, r_{dry} is the radial growth factor:

$$GF_r = \frac{r_{wet}}{r_{dry}} \quad \text{(S3)}$$

The GF_r of an equilibrated probe droplet is used to determine the RH using the E-AIM model, which accurately correlates these parameters for a range of inorganic aerosol, including NaCl.[9–11]

The upper and lower errors from determining the RH from a water probe droplet are:[1]

$$RH_w{}^{+\text{error}} = \left(0.169\, RH_w{}^2\right) - 0.364\, RH + 0.194 \quad \text{(S4a)}$$

$$RH_w{}^{-\text{error}} = -0.02\, RH + 0.21 \quad \text{(S4b)}$$

For an aqueous NaCl probe droplet the upper and lower errors in determining the RH are:[1]

$$RH_{NaCl}{}^{+\text{error}} = \left(-0.0199\, RH_{NaCl}{}^2\right) + 0.0130\, RH + 0.0063 \quad \text{(S5a)}$$

$$RH_{NaCl}{}^{-\text{error}} = \left(-0.0266\, RH_{NaCl}{}^2\right) + 0.0086\, RH + 0.0017 \quad \text{(S5b)}$$

Capacitance RH probes (e.g. Vaisala) can be used to record the RH to an accuracy that is typically between ±1% and ±3%. Both methods described here using a probe droplet to retrieve the gas phase RH are associated with a lower uncertainty in determining the gas RH.

To infer the hygroscopic response of a solute, the mass flux of evaporating sample-droplet is used with the gas-phase RH as determined from the drying kinetics of the probe-droplet. Equation S2 is rearranged to solve for a_w:

$$a_w = RH - \left[\frac{I\, R\, T_\infty}{2\, Sh\, \pi\, r\, M\, \beta_M\, D\, p^0(T_\infty) A}\right] \times \left[1 + \frac{I\, L^2\, M}{K\, R\, \beta_T\, T_\infty{}^2}\right]^{-1} \quad \text{(S6)}$$

The mass flux, I, can be estimated from the evaporation profile (radius vs. time) of the sample droplet. The radii data are converted into a mass using the droplet density, which is not known but can be estimated through numerical iterations, using a parameterisation of the density as a function of the $mfs^{1/2}$ and assuming a that the droplet is of homogeneous composition. Once the mfs vs. time has been retrieved, as well as the a_w vs. time, the mfs vs. a_w relationship can be determined, which is the aerosol hygroscopic response.

It is necessary to consider the evaporative cooling acting upon a droplet as this suppresses the vapour pressure of the solvent, which is particularly important at early times when the mass flux is greatest.

The droplet temperature can be estimated from the mass flux:[12]

$$T_{droplet} - T_{gas} = \frac{-I\, L}{4\, \pi\, \beta_T\, K\, r} \quad \text{(S7)}$$

The Kulmala model in Eq. S6 can only accurately simulate the mass flux of droplet evaporation under quasi-isothermal conditions, i.e. slow evaporation when the droplet temperature remains relatively constant (within 3 K of the gas phase). Typically, this process is repeated for 10 – 15 sample droplets at one constant RH, and then repeated at a range of RHs to determine the equilibrium hygroscopic response across a wide RH range.

2. Artificial saliva formulation

The artificial saliva formulation was reproduced from the procedure of Woo et al., (2010).[13] The final fluid composition is summarised on Table S1.

3. Surrogate deep lung fluid formulation

The lung fluid was prepared according to a modified procedure.[14] Briefly, DPPG (5 mg), 1.92 mL of DPPC (25 mg/mL solution in chloroform) and 5 uL of cholesterol solution (200 mg/mL in chloroform) were combined in a glass vial and dried under a nitrogen film until a thin dry lipid film was formed. The film was rehydrated with 4 mL of albumin (22 mg/mL), 4 mL of IgG (6.5 mg/mL) and 1 mL of transferrin (15 mg/mL), all solutions were prepared in pre-warmed HBSS at 55°C. Finally, 88.5 uL of glutathione (18.26 mM), 88.5 uL of sodium ascorbate (13.80 mM) and 88.5 88.5 uL of sodium urate (10.79 mM) were added and the rehydrated film was vortexed for 5 min. The lipids were dispersed by sonication over ice for 10 min (20% amplitude, 30 sec on, 30 sec off). Finally 10 uL of gentamicin (50 mg/mL) and 775 uL of HBSS were added. The mixture was stored in the fridge for up to 14 days/freeze dried. Portions of the freeze-dried samples were reconstituted with 2 mL DI water at different solute mass fractions and used for the droplet kinetic and the hygroscopicity measurements.

DPPG and DPPC were obtained from Avanti. Albumin (from human serum). IgG (reagent grade, from human serum) and transferrin (from human blood plasma) were obtained from Sigma, Other reagents were of technical grade and obtained from Sigma. The final fluid composition is summarised on Table S1.

Table S1: Compositions of artificial saliva and deep lung fluid.

Artificial Saliva	Concentration (g/L)	Surrogate Deep Lung Fluid	Concentration (g/L)
$MgCl_2$	0.04	DPPG	0.5
$CaCl_2.H_20$	0.013	DPPC	4.8
$NaHCO_3$	0.42	Cholesterol	0.1
0.2M KH_2PO_4	7.7 ml	Albumin	8.8
0.2M K_2HPO_4	12.3 ml	IgG	2.6
NH_4Cl	0.11	Transferrin	1.5
KSCN	0.19	Ascorbate	140 µM
$(NH_2)_2CO$ (urea)	0.12	Urate	95 µM
NaCl	0.88	Glutathione	170 µM
KCl	1.04	Gentamicin	10 µl
Mucin	3	HBSS	775 µl
DMEM	1 ml		
Alpha-amylase	-		
Deionised water	979 ml		

Abbreviations

DPPC	1,2-dipalmitoyl-sn-glycero-3-phosphocholine
DPPG	1,2-dipalmitoyl-sn-glycerol-3-phosphot-rac (1- Glycerol)
DMEM	Dulbecco's modified Eagle's medium
IgG	Immunoglobulin G
HBBS	Hank's balanced salt solution
NaCl	Sodium Chloride
$MgCL_2$	Magnesium chloride
$CaCl_2$	Calcium chloride
$NaHCO_3$	Sodium bicarbonate
KH_2PO_4	Monopotassium phosphate
K_2HPO_4	Dipotassium phosphate
NH_4Cl	Ammonium chloride
KSCN	Potassium thiocyanate
KCl	Potassium chloride

4. The Evaporation-Sedimentation Model

The evaporation-sedimentation model used here follows the framework of Xie et al., (2007),[15] using the respiratory jet treatment of Liu et al., (2017).[16] The parameterisations for the latent heat and equilibrium vapour pressure of water are from Su (2018),[17] water density from Wagner (1993),[8] viscosity & thermal conductivity of air and water vapour diffusion coefficient are from Miles (2012),[18] and air density from Picard (2008).[19] The parameterisations for density, mass fraction of solute (Table S2) and hygroscopicity for saliva and deep lung fluid are derived from novel measurements for this publication. Thermodynamic treatments for NaCl are taken from the Extended Aerosol Inorganics Model (E-AIM) and hygroscopicity value $\kappa = 1.2$.

Table S2: The modelled relationship between a_w, MFS and density for saliva and deep lung fluid droplets derived from EDB measurements.

$$MFS = a + (b \times a_w^{1}) + (c \times a_w^{2}) + (d \times a_w^{3}) + (e \times a_w^{4}) + (f \times a_w^{5})$$

$$Density = g + (h \times MFS^{0.5}) + (i \times MFS^{1}) + (j \times MFS^{1.5})$$

	a	***b***	***c***	***d***	***e***	***f***
Saliva	1	0.13414	-4.73918	10.23153	-6.62626	0
DLF	0.9882	-0.41457	0.08651	-3.41587	8.81332	-6.05769
	g	***h***	***i***	***j***		
Saliva	995.78	262.92	-606.15	1135.53		
DLF	997	-43.88148	397.75347	-100.99474		

5. Extended Results

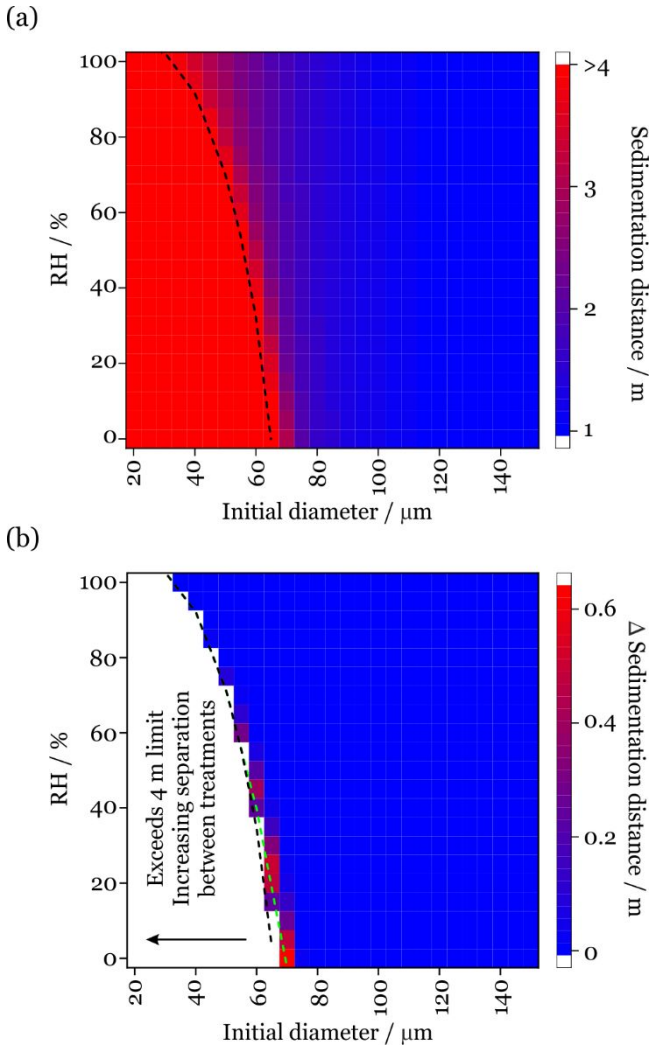

Fig. S2: (a) The sedimentation distance for deep lung fluid droplets projected from a cough at 10 m/s into an environment at 293 K. The black dashed line indicates when the 4 m sedimentation limit is reached. (b) The change in sedimentation distance on assuming the droplets are composed of sodium chloride solution rather than deep lung fluid. The dashed lines indicate when the 4 m sedimentation limit is reached for saliva (black) and NaCl (green).

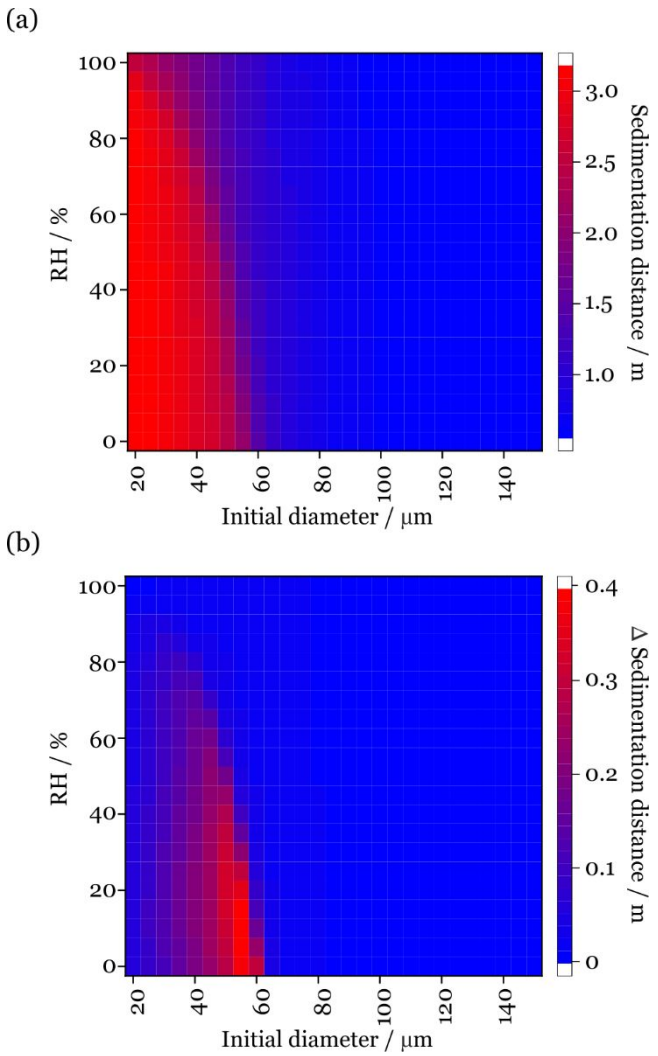

Fig. S3: (a) The sedimentation distance for saliva droplets project from speaking at 5 m/s into an environment at 293 K. (b) The change in sedimentation distance on assuming the droplets are composed of sodium chloride solution rather than saliva.

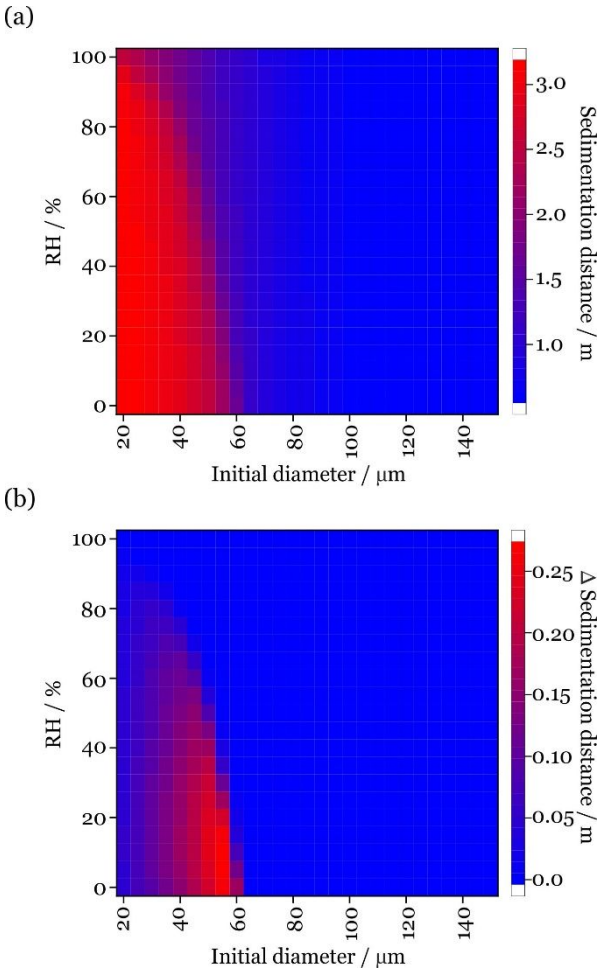

Fig. S4: (a) The sedimentation distance for deep lung fluid droplets project from speaking at 5 m/s into an environment at 293 K. (b) The change in sedimentation distance on assuming the droplets are composed of sodium chloride solution rather than deep lung fluid.

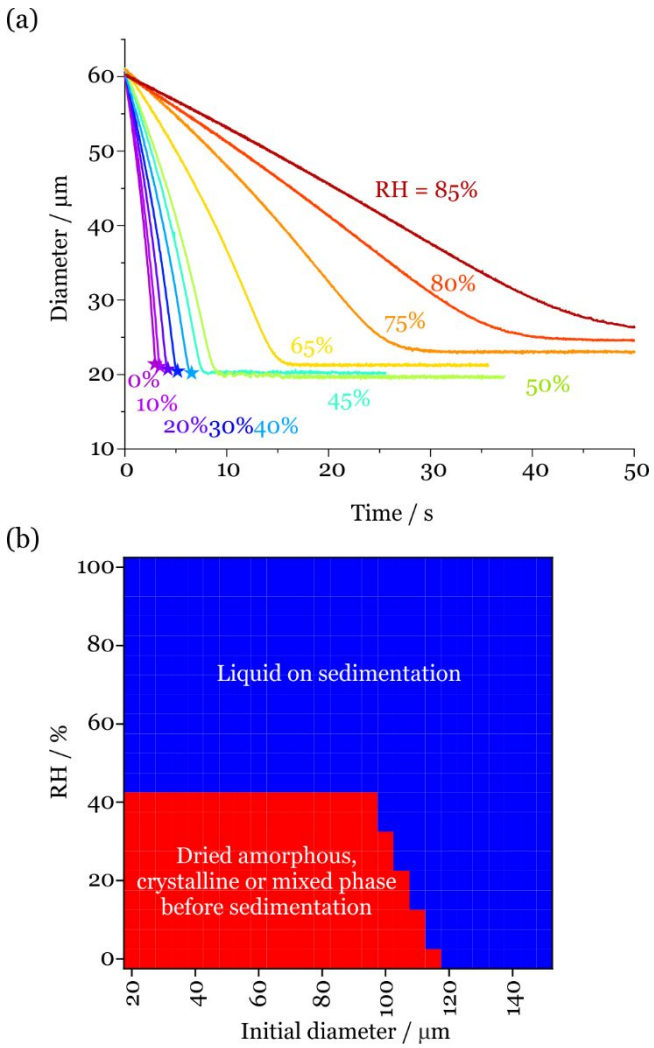

Fig. S5: Evaporation kinetics of surrogate saliva droplets with varying RH. The stars identify the onset of disruption to the light scattering pattern, indicating a phase change has occurred to a non-spherical particle morphology. (b) Phase identification of drying saliva droplets with varying droplet size and RH. The red bounded region indicates that droplets undergo a phase change before sedimenting onto a surface.

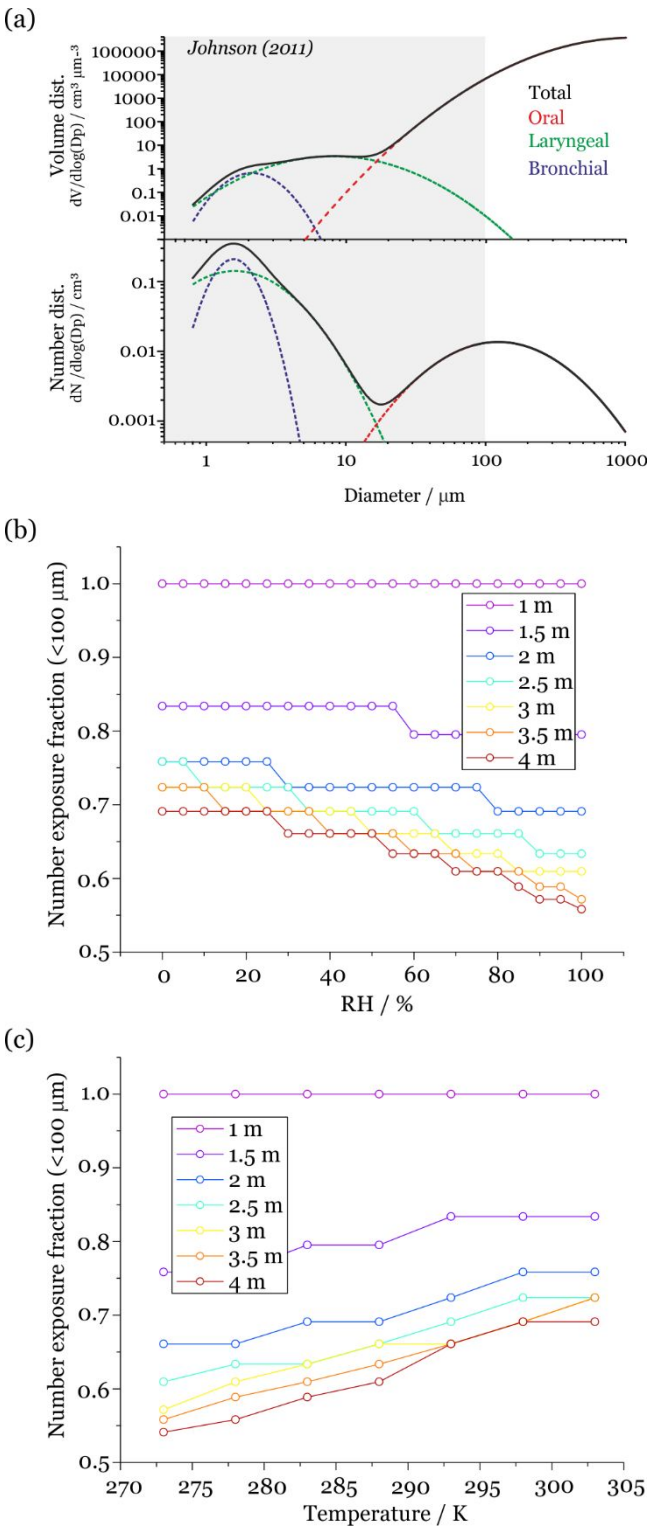

Fig. S6: (a) Respiratory fluid droplet distributions from Johnson et al. (2011) for a cough.[20] The grey region represents the < 100 µm diameter range. (b) The RH dependent droplet number exposure fraction at 1, 1.5, 2, 2.5, 3, 3.5 & 4 m for saliva droplets in the initial diameter range < 100 µm. (c) The temperature dependent droplet number exposure fraction at 1, 1.5, 2, 2.5, 3, 3.5 & 4 m for saliva droplets in the initial diameter range < 100 µm.

References

(1) Rovelli, G.; Miles, R. E. H.; Reid, J. P.; Clegg, S. L. Accurate Measurements of Aerosol Hygroscopic Growth over a Wide Range in Relative Humidity. *J. Phys. Chem. A* **2016**, *120* (25). https://doi.org/10.1021/acs.jpca.6b04194.

(2) Marsh, A.; Miles, R. E. H.; Rovelli, G.; Cowling, A. G.; Nandy, L.; Dutcher, C. S.; Reid, J. P. Influence of Organic Compound Functionality on Aerosol Hygroscopicity: Dicarboxylic Acids, Alkyl-Substituents, Sugars and Amino Acids. *Atmos. Chem. Phys.* **2017**, *17*, 5583–5599.

(3) Marsh, A.; Rovelli, G.; Miles, R. E. H.; Reid, J. P. Complexity of Measuring and Representing the Hygroscopicity of Mixed Component Aerosol. *J. Phys. Chem. A* **2019**, *123*, 1648–1660.

(4) Davies, J. F.; Haddrell, A. E.; Reid, J. P. Time-Resolved Measurements of the Evaporation of Volatile Components from Single Aerosol Droplets. *Aerosol Sci. Technol.* **2012**, *46*, 666–677.

(5) Gregson, F. K. A.; Robinson, J. F.; Miles, R. E. H.; Royall, C. P.; Reid, J. P. Drying Kinetics of Salt Solution Droplets: Water Evaporation Rates and Crystallization. *J. Phys. Chem. B* **2019**, *123*, 266–276.

(6) Liu, Y.; Daum, P. H. Relationship of Refractive Index to Mass Density and Self-Consistency of Mixing Rules for Multicomponent Mixtures like Ambient Aerosols. **2008**, *39*, 974–986.

(7) Cotterell, M. I.; Mason, B. J.; Preston, T. C.; Orr-Ewing, A. J.; Reid, J. P. Optical Extinction Efficiency Measurements on Fine and Accumulation Mode Aerosol Using Single Particle Cavity Ring-down Spectroscopy. *Phys. Chem. Chem. Phys.* **2015**, *17* (24), 15843–15856. https://doi.org/10.1039/c5cp00252d.

(8) Kulmala, M.; Vesala, T.; Wagner, P. An Analytical Expression for the Rate of Binary Condensational Particle Growth. *Proc. R. Soc. Lond. A* **1993**, *441*, 589–605.

(9) Clegg, S. L.; Brimblecombe, P.; Wexler, A. S. Thermodynamic Model of the System H+ - NH4+ - Na+ - SO42- - NO3- - Cl- - H2O at 298.15 K. *J. Phys. Chem. A* **1998**, *102*, 2155–2171.

(10) Wexler, A. S.; Clegg, S. L. Atmospheric Aerosol Models for Systems Including the Ions H+, NH4+, Na+, SO42−, NO3−, Cl−, Br− and H2O. *J. Geophys. Res.* **2002**, *107*, 4207–4221.

(11) Clegg, S. L.; Brimblecombe, P.; Wexler, A. S. Thermodynamic Model of the System H+-NH4+-SO42-NO 3--H2O at Tropospheric Temperatures. *J. Phys. Chem. A* **1998**, *102*, 2137–2154.

(12) Archer, J.; Walker, J. S.; Gregson, F. K. A.; Hardy, D. A.; Reid, J. P. Drying Kinetics and Particle Formation from Dilute Colloidal Suspensions in Aerosol Droplets. *Langmuir* **2020**. https://doi.org/10.1021/acs.langmuir.0c01830.

(13) Woo, M. H.; Hsu, Y. M.; Wu, C. Y.; Heimbuch, B.; Wander, J. Method for Contamination of

Filtering Facepiece Respirators by Deposition of MS2 Viral Aerosols. *J. Aerosol Sci.* **2010**, *41* (10), 944–952. https://doi.org/10.1016/j.jaerosci.2010.07.003.

(14) Hassoun, M.; Royall, P. G.; Parry, M.; Harvey, R. D.; Forbes, B. Design and Development of a Biorelevant Simulated Human Lung Fluid. *J. Drug Deliv. Sci. Technol.* **2018**, *47*, 485–491. https://doi.org/10.1016/j.jddst.2018.08.006.

(15) Xie, X.; Li, Y.; Chwang, A. T. Y.; Ho, P. L.; Seto, W. H. How Far Droplets Can Move in Indoor Environments ? Revisiting the Wells Evaporation?Falling Curve. *Indoor Air* **2007**, *17* (3), 211–225. https://doi.org/10.1111/j.1600-0668.2007.00469.x.

(16) Liu, L.; Wei, J.; Li, Y.; Ooi, A. Evaporation and Dispersion of Respiratory Droplets from Coughing. *Indoor Air* **2017**, *27* (1), 179–190. https://doi.org/10.1111/ina.12297.

(17) Su, Y. Y.; Miles, R. E. H.; Li, Z. M.; Reid, J. P.; Xu, J. The Evaporation Kinetics of Pure Water Droplets at Varying Drying Rates and the Use of Evaporation Rates to Infer the Gas Phase Relative Humidity. *Phys. Chem. Chem. Phys.* **2018**, *20* (36). https://doi.org/10.1039/c8cp05250f.

(18) Miles, R. E. H.; Reid, J. P.; Riipinen, I. Comparison of Approaches for Measuring the Mass Accommodation Coefficient for the Condensation of Water and Sensitivities to Uncertainties in Thermophysical Properties. *J. Phys. Chem. A* **2012**, *116* (44), 10810–10825. https://doi.org/10.1021/jp3083858.

(19) Picard, A.; Davis, R. S.; Gläser, M.; Fujii, K. Revised Formula for the Density of Moist Air (CIPM-2007). *IOP Publ. Metrol. Metrol.* **2008**, *45*, 149–155. https://doi.org/10.1088/0026-1394/45/2/004.

(20) Johnson, G. R.; Morawska, L.; Ristovski, Z. D.; Hargreaves, M.; Mengersen, K.; Chao, C. Y. H.; Wan, M. P.; Li, Y.; Xie, X.; Katoshevski, D.; Corbett, S. Modality of Human Expired Aerosol Size Distributions. *J. Aerosol Sci.* **2011**, *42* (12), 839–851. https://doi.org/10.1016/j.jaerosci.2011.07.009.